Heliyon 9 (2023) e19708

Contents lists available at ScienceDirect

Heliyon

journal homepage: www.cell.com/heliyon

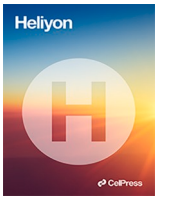

Influence of heat input on the mechanical characteristics, corrosion and microstructure of ASTM A36 steel welded by GTAW technique

S. Senthilkumar [a], S. Manivannan [b], R. Venkatesh [c], M. Karthikeyan [d,*]

[a] Department of Mechanical Engineering, Madha Engineering College, Kundrathur, Chennai, Tamilnadu, 600069, India
[b] Centre for Material Science, Department of Mechanical Engineering, Karpagam Academy of Higher Education, Coimbatore, Tamil Nadu, 641021, India
[c] Department of Mechanical Engineering, Saveetha School of Engineering, SIMATS, Chennai, Tamil Nadu, 602105, India
[d] Department of Electrical and Computer Engineering, Wolaita Sodo University, Sodo, Ethiopia

ARTICLE INFO

Keywords:
ASTM A36 steel
Gas tungsten arc welding
Microstructure
Tensile
Hardness
Corrosion test

ABSTRACT

The Gas Tungsten Arc Welding process weld for the 4 mm thickness of the ASTM A36 steel plate with varied heat input parameters of 0.608 kJ/mm, 0.900 kJ/mm and 1.466 kJ/mm, respectively. The effect of different heat inputs on microstructure, corrosion, and mechanical characteristics of developed weld joints are examined by three zones: heat-affected zone, welded zone, and base metal zone. The optical microscopic results of weld joints illustrate that fine grain structure leads to enhance welding strength. It is revealed that the increased heat input parameter on the weld joint shows a decreased tensile strength and hardness of the weld joint. The corrosion resistance of the weld joint is evaluated by Potentio-dynamic polarization. It facilitates that the corrosion rate of the weld joint is decreased with increasing heat input, which results indicate the best and worst corrosion micrograph of the polygonal ferrite and ferrite plus polygonal ferrite. However, the weld joint prepared with 0.900 kJ/mm heat input found maximum corrosion resistance.

1. Introduction

The utilization of welding products are gradually increased in our routine life. It offered various applications like vehicles, bridges, power generation equipment, buildings, etc. welding definition represented by the American welding society localized coalescence of non-metals or metals joined by heating the materials to a welding temperature with or without the application of pressure or by the application of pressure alone and with or without the use of filler metal. Welding processes can be broadly divided into fusion welding process and solid state welding process. Metals are joined by heating to their melting point in fusion welding, whereas in a solid state, welding occurs at a temperature that is at least the material's melting temperature. However, it has its advantages and disadvantages. Fusion welding processes are well established and extensively used worldwide because of their capability to produce high-quality joints with much ease and low setup and labour cost [1]. Change in metallurgical properties of the materials while welding, difficulty in joining dissimilar materials and environmental-related problems are some of the negative aspects of fusion welding processes.

* Corresponding author.
E-mail addresses: drssk.print@gmail.com (S. Senthilkumar), manivannan.s@kahedu.edu.in (S. Manivannan), venkidsec@gmail.com (R. Venkatesh), karthikeyan.m@wsu.edu.et (M. Karthikeyan).

https://doi.org/10.1016/j.heliyon.2023.e19708
Received 21 March 2023; Received in revised form 3 May 2023; Accepted 30 August 2023
Available online 1 September 2023

Solid-state welding is free of these problems and gives excellent welds [2]. Commonly, stainless steel is familiar to resist rust formation against corrosion. The chromium oxide film coating applied over the steel surfaces offers good prevention against corrosion in the caustic environment [3,4]. Mostly, Austenitic stainless steel is utilized by various marine applications due to its stability ina high corrosion environment [5–7].

Moreover, the Austenitic stainless steel was more sensitive to chloride immersion, which leads to increased stress corrosion-based cracking [8]. The selection of appropriate stainless steel combination, processing of metals on different thermal and mechanical conditions, and duplex stainless steel join has facilitated dual phase microstructure like austenite/ferrite results in increased mechanical strength of metal joint [9–12]. The experimental study of corrosion characteristics on ×65 steel under CO_2 saturation with water content base and the combinations of acetic acid evaluated via the electrochemical method, localized electrochemical impedance spectroscopy (LEIS), surface analysis, and scanning vibrating micro-electrode (SVME). It was observed that the steel was in an active state of dissolution on Fe dominates during the water immersion. The intermediate product adsorption of electrode and weld surfaces found an inductive loop field on the lower frequency series plot of EIS. It noted that the concentrations of corrosion increased. Similarly, [Fe 2+] × [CO_3 2-] was found over solubility on the deposit of $FeCO_3$ electrode surface, preventing the steel from additional corrosion. However, the passive state, that the electrode surfaces were wrapped with the film of $FeCO_3$ disappeared the low frequency on the inductive loop. Moreover, the existence of an acetic acid combination with water has enhanced the resistance of corrosion as well as limits the reduction of undiscounted acetic acid [13,14].

Electrochemical and weight loss techniques evaluated the corrosion performance of mild steel. An electrochemical method consisting of CH_3COOH and CO_2 base solution has to affect the cathode terminal. Similarly, the effect of acetic acid on the corrosion rate of weld joints tested under elevated temperatures was found to be high concentrations. The acetic acid in the form of un dissociated observed in less pH, Which has increased the corrosion rate [15]. They attempt to evaluate the corrosion behaviour of static simulated produced water (SPW) saturated on 3 pipeline steel under supercritical atmospheric conditions of CO_2 via a weight loss route. Various XPS, XRD, and SEM techniques were used to find the corroded micrograph surfaces. The test results of corrosion rate were decreased progressively with increased temperature under static saturated SC/CO_2. The inhomogeneous calcium and iron distribution of elements observed in the weld surface film. The formation of $FeCaCo_3$ has due to lower temperatures [16].

Three kinds of microstructure have been attained by the welding joint of carbon steel corrosion resistance was evaluated via an electrochemical route under the simulated conditions of water/CO_2 with an applied temperature of 90 °C. The micrograph results of weld joint metal found uniform ferrite grains with polygonal, acicular ferrite structure with few pearlite grains. The above electrochemical system consists of spectroscopy, linear polarization resistance, and potentiodynamic polarization and offers corrosion studies. It reveals that the joint with a polygonal ferrite structure found optimum corrosion resistance compared to all others. It was due to their high heat input supply during the welding process [17].

Low-carbon martensitic stainless steel (13/4) has been utilized in hydro turbine applications due to its enhanced corrosion resistance and strength. The salt nature may corrode the material. It leads to silt erosion and offers damage tothe turbine blade. So that the welding operation may help to overcome the above deficiency. They experimentally studied its weld joint heat-affected zone (HAZ) characteristics via a thermal simulator. Similarly, the mechanical behaviour was evaluated and compared the test results with standard samples. The weld joint on HAZ was found to have maximum impact toughness and ductility of 52.8 J and 19.3% under 1000 °C. Similarly, the microstructure of weld samples has been observed at different weld zone [18]. Therefore, the ASTM 36 steel plate is welded by GTAW technique with varied heat inputs (0.608 kJ/mm, 0.900 kJ/mm and 1.466 kJ/mm). The welded plates were subjected to microstructural, corrosion, and mechanical properties. It was revealed that the improvement in heat input results reduced corrosion and mechanical performance compared to low heat input. Moreover, the low heat input offered good microstrucal bonding, corrosion and tensile behaviour.

2. Material and principles

2.1. Material selection

The most common structural steel ASTM A36 is chosen for this investigation. Its machinability rate is 72%, with an average feed rate of 120 ft/min [9]. The material can weld easily through oxyacetylene welding, gas metal arc welding (GMAW), and shield metal arc welding (SMAW), which offers good quality weld joints in structural applications [17,18]. The chemical compositions and mechanical properties of ASTM A36 steel are mentioned in Table s 1 and 2, respectively.

2.2. Principle of GTAW

It is the one type of advanced welding technique that offers the tungsten inert gas (TIG), which consists of a tungsten (non-consumable) electrode, which has to produce the arc between the metals and form the weld joint. The inert gas (Argon/helium) has to

Table 1
Chemical compositions of ASTM A36 steel.

Fe	C	Mn	Si	Cu	S	P
98.0%	0.27%	1.03%	0.28%	0.20%	0.050%	0.040%

Table 2
Mechanical characteristics.

Properties	Strength		Elongation at break		Modulus of elasticity	Shear modulus	Bulk Modulus	Poisson's ratio
	Tensile	Yield	200 mm	50 mm				
Units	MPa		%		GPa			–
Value	500	250	20	23	200	79.3	140	0.26

prevent oxidation during the welding process and the filler rod is used correspondingly in the welding area. The non-consumable tungsten electrode fused by high heat energy supplied via an electrical source and arc produced between the metal surfaces is melted and joined together through a filler rod. It makes an effective weld joint between similar or dissimilar metal surfaces. The filler material has been varied due to the selection of base metals. During the welding process, shield gas is to be provided on the field of weld zone, tungsten electrode, and molten metal zone to eliminate the chemical integrity. Among the various welding techniques, the GTAW is mainly utilized to join dissimilar metal combinations as non-ferrous metal (aluminium, copper, and magnesium alloys) to stainless steel. The process of computing the shield and GTAW to facilitates high-quality strong welding. Based on the metal thickness, the amps rating is fixed to perform the effective GTAW process on different polarity like alternative current (AC), direct current reverse (DCRP), and straight polarity (DCSP), respectively.

2.3. Experimental details

The actual experimental setup of GTAW or TIG is shown in Fig. 1. It consists of three different stages. The first stage of TIG welding considers the ASTM A36 steel plate with 4 mm thickness under different welding parameters like welding speed range and current. The second stage welding process uses a mild steel plate of 5 mm thickness. The last third stage was performed with variations of welding input parameters that could provide the optimum heat input compared to the second stage. The current variations have performed it and voltage leads to decreased weld speed and increased input heat.

The current investigation selects the autogenous TIG welding arrangements performed with a constant velocity of filler movement during the welding process. The welding equipment consists of a work holding device, inert gas supply unit, power supply, electrode, and welding torch. The TIG torch is held above the work materials and maintains a constant distance to produce an effective arc.

2.4. ASTM A36 steel plate – autogenous (single pass) TIG welding operation

The ASTM A36 steel plate 4 mm thick is welded by autogenous (single phase) TIG welding with filler material. Initially, the ASTM A36 steel plate was cut into 100 mm × 50 mm x 4 mm and then steel plate edges were polished with different grades of silicon carbide emery sheets until the grinding polish was applied. Finally, the dust and unwanted metal particles are removed and provide the required surface finish. The prepared steel plates are fixed into the welding table and an electrical DC supply is applied between the polarities. The 2.4 mm diameter tungsten electrode with varied current and speed is mentioned in Table s 3 and 4,respectively. The welded ASTM A36 steel sample with different heat inputs is shown in Fig. 2.

2.5. Preparation of test sample

The ASTM A36 welded steel joint is cut at a transverse direction of weldment as the size of 20 mm × 10 mm and different silicon carbide emery sheets are polished. It continued with fine glass polish to help identify different structures. The prepared test sample microstructure is studied via optical microstructure with different ranges. It helps to detect the various micrograph as well as micro

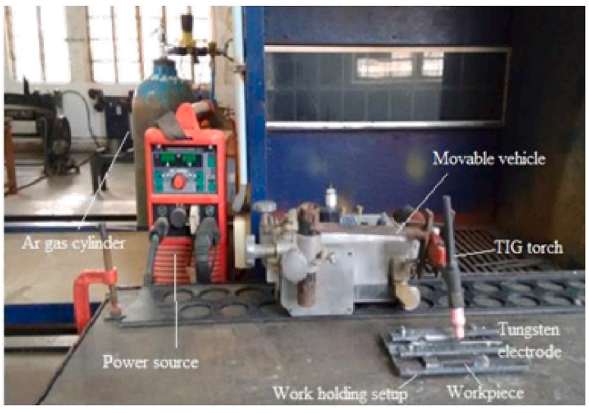

Fig. 1. Actual experimental setup of GTAW.

Table 3
Basic details of TIG welding.

Dimensions of the Steel	100 mm × 50 mm x 4 mm
Gas Flow Rate	12 L/min
Mode of current	DCEN
Weld centre to Electrode tip Distance	3 mm
Shield gas	Argon

Table 4
Parameters of the welding process.

Parameters	Units	Weld joint-1	Weld Joint-2	Weld Joint-3
Current	Amps	160	180	200
Voltage	Volts	19	20	22
Speed	mm/sec	5	4	3
Heat Input	kJ/mm	0.608	0.9	1.466

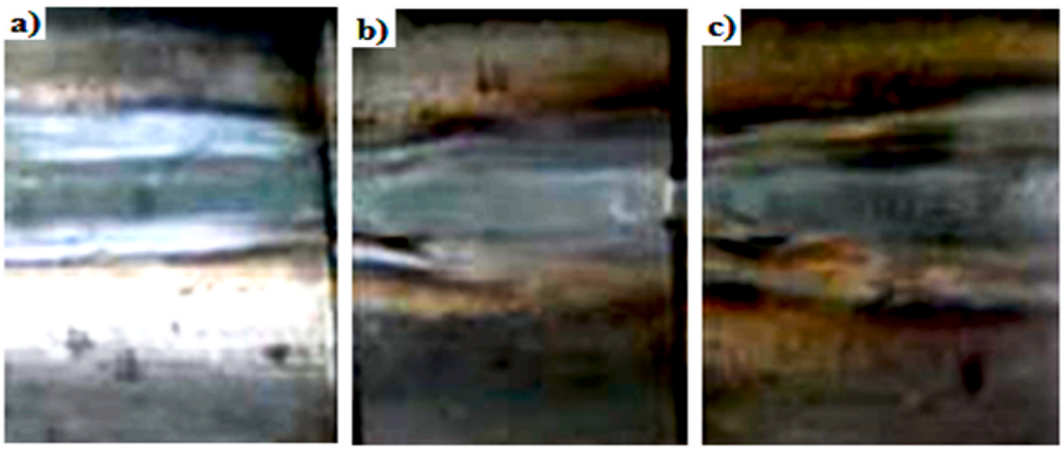

Fig. 2. Welded Samples of different heat input a) 0.608 kJ/mm, b) 0.900 kJ/mm, and c) 1.466 kJ/mm.

cracks.

Based on the ASTM E8 standard, the tensile test sample is prepared by I shape via wire cut EDM apparatus, shown in Fig. 3. The developed tensile test samples are evaluated by Instron make universal tensile testing machine configured with 600 KN load.

The micro Vickers hardness of weldment, heat affected zone (HAZ) and nearer to the weld zone is evaluated by diamond tip indentation of 500 gms applied load at 50sec.

3. Results and discussion

3.1. Microscopic studies

The effect of heat input on weld depth penetration is examined across the weldment. It consists of the base metal zone (BMZ), welded zone (WZ), and heat affected zone (HAZ), as represented in Fig. 4 and the test samples are carefully examined for their internal microstructure via an optical microscope. The microscopic images of ASTM A36 welded steel joint with 0.608 kJ/mm, 0.900 kJ/mm, and 1.466 kJ/mm heat input is shown in Figs. 5–7.

3.1.1. Weld Joint-1(Heat Input-0.608 kJ/mm)

Fig. 5(a–c) illustrates the optical micrograph of the different zone on welded ASTM A36 steel joint sample prepared by 0.608 kJ/

Fig. 3. Tensile test sample.

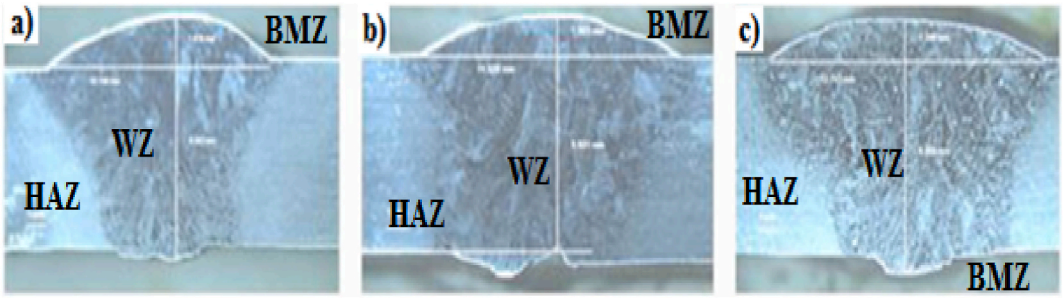

Fig. 4. Cross sections of the Weld Joints with different heat inputs a) 0.608 kJ/mm, b) 0.900 kJ/mm, and c) 1.466 kJ/mm.

mm heat input.

Fig. 5 (a) illustrates the microstructure of the base metal zone on welded ASTM A36 steel under the heat input of 0.608 kJ/mm. The varied grain size is observed with ferrite steel structure. While the GTAW process with 0.608 kJ/mm heat input formed the ASTM A36 steel joint, the Acicular ferrite structure with uniform enlarged, grain distribution is illustrated in Fig. 5 (b). The weld joint consisting of fine uniform grain size has been increasing the quality of the joint [2]. It helps to increase the join fusibility and improve the composite's mechanical strength. The nearby welded metal on the heat-affected zone has a moderate grain structure. It consists of a ferrite and austenitic structure that offers weld stability during high thermal input. The structure of heat affected zone on ASTM A36 steel weld is shown in Fig. 6 (c).

3.1.2. Weld Joint-2 (heat Input-0.900 kJ/mm)

The optical microscope images of the different zone on the ASTM A36 welded steel sample developed with 0.900 kJ/mm heat input is shown in Fig. 6(a and b).

Fig. 6 (a) illustrates the microstructure of welded zone (WZ) on ASTM A36 steel weld under the heat input of 0.900 kJ/mm. It was observed from Fig. 6 (a) that the combinations of polygonal ferrite and acicular ferrite structure were formed during the GTAW process under increased heat input of 0.900 kJ/mm. The structure may lead to withstand the high tensile force and results in increased elongation properties. Similarly, the microstructure of heat affected zone (HAZ) on the ASTM A36 steel joint is represented in Fig. 6 (b). The figure illustrates that the various fine-dotted coarse grain structure offers good thermal stability. Significant microstructure changes are found on the 0.900 kJ/mm heat input. However, the higher heat input enhances the metal pool quality and reduces the formation of polygonal ferrite structure [11,12].

3.1.3. Weld Joint-3 (heat Input-1.446 kJ/mm)

The optical microscopic micrograph of the welded and heat-affected zones on the ASTM A36 welded steel sample prepared by 1.466 kJ/mm heat input is shown in Fig. 7(a and b). It is noted from Fig. 7 (a) that the polygonal ferrite structure formations are identified with multi-directional non-uninformed grains facilitating a small amount of internal welding crack. It has to minimize the mechanical strength of the weld joint.

Fig. 7 (b) shows the enlarged coarse ferrite grain structure. It is formed by high heat input of 1.466 kJ/mm on the GTAW process. The area of ASTM A36 steel is mainly affected by high heat input of 1.466 kJ/mm, as proved in Fig. 7 (b).

3.2. Mechanical behaviour studies

3.2.1. Study of micro Vickers hardness of weld joint

The micro-Vickers hardness of GTAW welded ASTM A36 steel is evaluated by three different places base metal (BM), welded metal (WM), and heat affected zone (HAZ). The experimental result value of micro Vickers hardness on welded ASTM A36 steel joint is mentioned in Table .5.

Fig. 8 represents the micro Vickers hardness value of welded ASTM A36 test sample. It is noted that the hardness of the weld joint is decreased with an increase in heat input from 0.608 kJ/mm to 1.466 kJ/mm. It was due to their changes in internal microstructure. It facilitates to decrease in mechanical behaviour. The weld joint 1 operated under 0.608 kJ/mm, found a maximum hardness of 187Hv and improved by 22% compared to weld joint 3. It is observed that the hardness of welded ASTM A36 is increased by the subsequent order of HAZ/weld metal zone/base metal. Weld joints 2 and 3 found decreased hardness values of 168Hv and 153Hv on the welded metal zone. The decreased hardness of value is due to the formation of non-uninformed grains that facilitates the micro welding cracks. It is proved in Fig. 6 (b) and 7 (b), respectively.

3.2.2. Study of tensile strength of weld joint

The tensile test samples of ASTM A36 steel welded with different heat input conditions are evaluated and compared with the base metal. Each heat input's three test samples are evaluated and its average tensile strength is considered. Table .6 shows the tensile strength results of the weld mentioned above samples.

Fig. 9 shows the tensile strength of different ASTM A36 weld joints prepared by 0.608 kJ/mm, 0.900 kJ/mm and 1.466 kJ/mm.

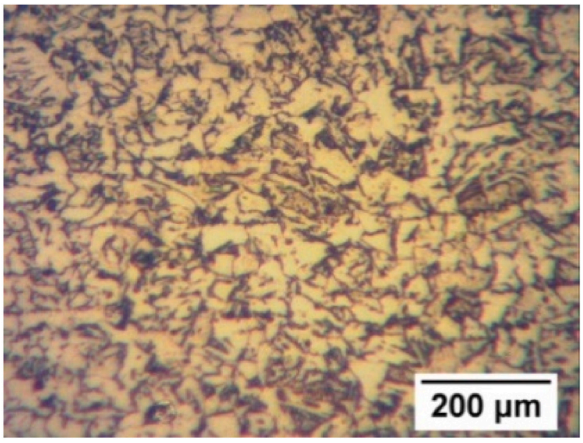

(a) Base metal

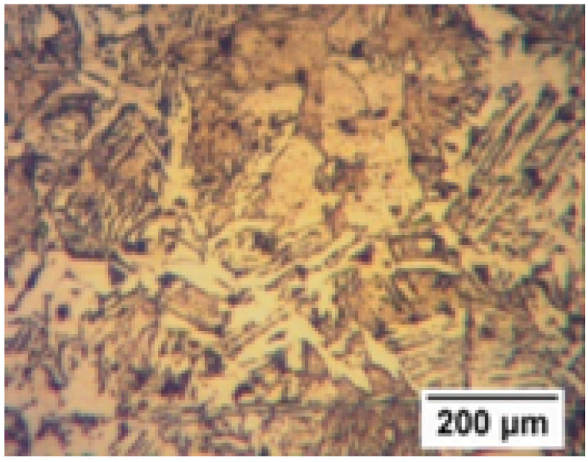

(b) Welded zone @ 0.608KJ/mm

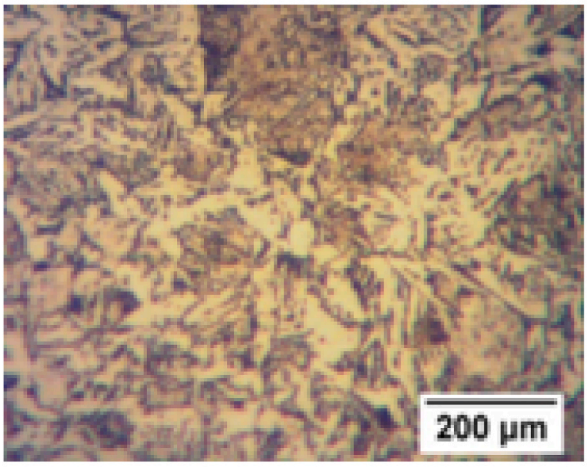

(c) Heat affected zone @ 0.608KJ/mm

Fig. 5. (a) Base metal
(b) Welded zone @ 0.608 kJ/mm
(c) Heat affected zone @ 0.608 kJ/mm.

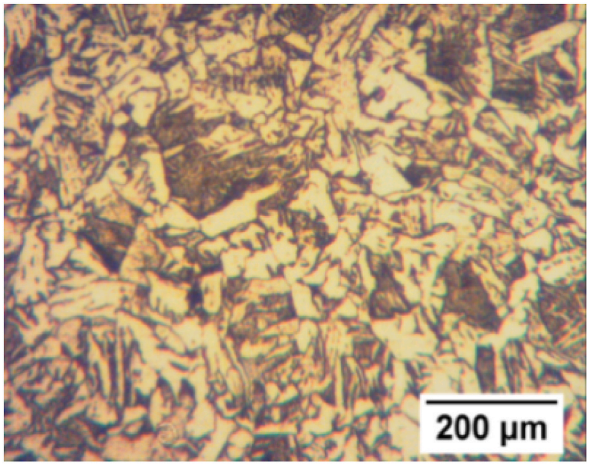

Fig. 6. (a) Welded zone @ 0.900 kJ/mm
(b) Heat affected zone @ 0.900 kJ/mm.

Heat input. It is revealed from Fig. 9 that the tensile strength of the weld joint is increased with decreased heat input. The maximum tensile strength of 483 MPa is found on 0.608 kJ/mm heat input and is improved by 3% compared to weld joint 3. The improved tensile strength is due to forming of an acicular ferrite structure with uniform grain distribution. It is evidenced in Fig. 6 (b). So, weld joint 1 reveals that the joint prepared with max current and least weld speed having good tensile strength is shown in Fig. 9.

3.3. Electrochemical corrosion test

Fig. 10 represents the experimental setup of Potentio dynamic Polarization on welded ASTM A36 steel corrosion resistance. A sample of size 20mm × 20 mm is prepared such that the test surface should arrest the hole of the PDP equipment, as shown in Fig. 11 The corrosion test results of the welded sample are mentioned in Table .7. The variations in the corrosion behaviour of test samples with different heat input conditions are shown in Figs. 12 and 13.

The present experimental corrosion study is considering for platinum counter electrode with the reference of Ag/AgCl probe in 1 M KCL solution (Calomel electrode). The weld plates are sized by 200 mm × 200 mm and investigated by Potential dynamic polarization with NaCl solution.

Fig. 12 represents the Potential vs Current Density graph of the corrosion study on ASTM A36 welded joint with different heat inputs.

From the above graph, it is observed that the current density of the given samples is in the increasing order of Blue < Pink < Black. Black -Weld Joint-1, Pink -Weld Joint-2, and Black -Weld Joint-3

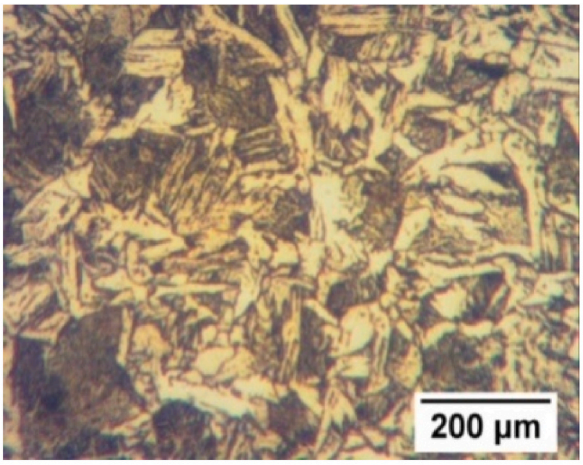

(a) Welded zone @ 1.466 kJ/mm

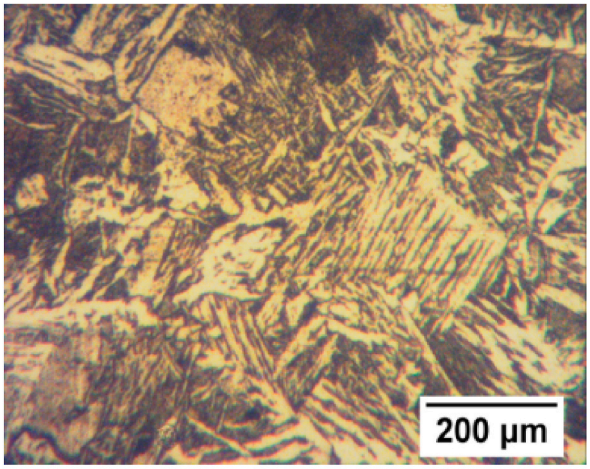

(b) Heat affected zone @ 1.466 kJ/mm

Fig. 7. (a) Welded zone @ 1.466 kJ/mm
(b) Heat affected zone @ 1.466 kJ/mm.

Table 5
Micro-Vickers hardness of welded ASTM A36 sample with different zone.

Weld Joint/Descriptions	Heat Input	Vickers hardness number		
		BM	WM	HAZ
	in kJ/mm	in Hv		
Weld Joint-1	0.608	190	187	179
Weld Joint-2	0.900	190	168	154
Weld Joint-3	1.466	190	153	141

$$Corrosion\ rate, CR = i_{corr}\frac{kW}{AD} \quad (1)$$

I_{corr} = Current at corrosion (Amp)
K = Constant
W = Equivalent Weight (gm/mol)
A = Area exposed to corrosion (cm^2)

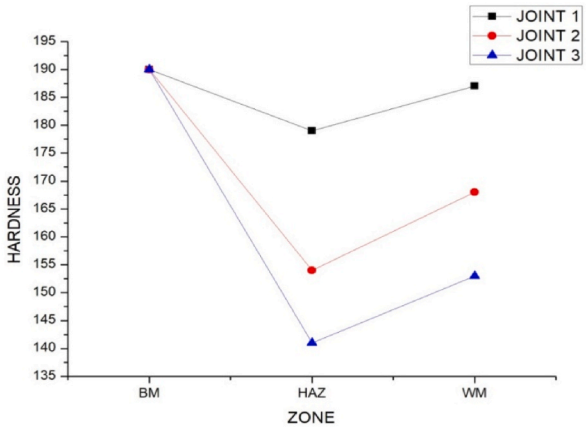

Fig. 8. Micro Vickers hardness number.

Table 6
Tensile test results.

Weld Joint	Heat Input (kJ/mm)	Tensile Strength (MPa)
Weld Joint-1	0.608	483
Weld Joint-2	0.900	475
Weld Joint-3	1.466	468

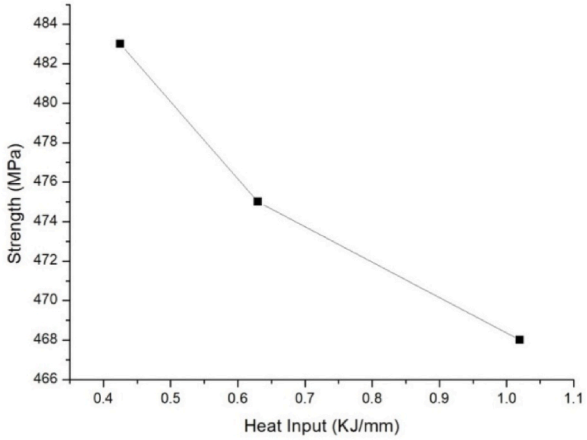

Fig. 9. Tensile strength of weld joints.

D = Density (gm/cm^3)

Fig. 13 illustrates the corrosion rate of ASTM A36 steel welded joints with various heat inputs. It is observed that the corrosion rate decreases with an increase in the heat input. It means corrosion resistance increases with an increase in the heat input due to the change in grain morphology from acicular ferrite to polygonal ferrite. The phase changes during the weld joint on different heat inputs are represented in Figs. 5–7. The weld joint 3 with higher heat input found a minimum corrosion rate of 0.0902 mm/year. The other joints found an increased corrosion rate of 0.2795 mm/year and 0.3825 mm/year, respectively.

4. Conclusions

The heat input had a more significant influence on both the mechanical and corrosion properties ofASTM A36 Steel Welded by GTAW. The grain size increases with the heat input in the weld zone and HAZ due to the change in cooling rate. The hardness decreases with an increase in heat input due to the change in grain size. The strength is also affected similarly to hardness. The corrosion rate decreases with increasing heat input due to the formation of Polygonal ferrite at the expense of acicular ferrite. The heat input should be optimized to produce a sound weld for better mechanical and corrosion properties. The parameters used in weld joint-2 are suggested for welding 4 mm ASTM A36 steel material with the TIG welding process suitable for caustic marine applications.

Fig. 10. Actual experimental setup for Potentio dynamic polarization.

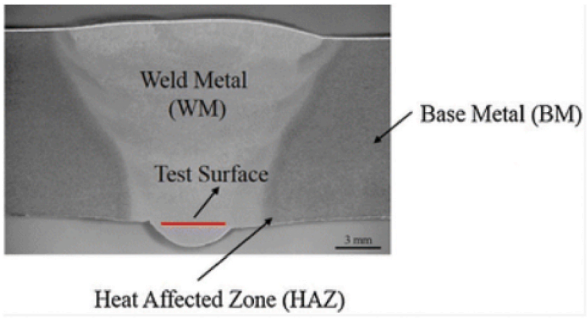

Fig. 11. Test position in the weld joints.

Table 7
PDP Test results.

Weld Joint	Heat Input (kJ/mm)	Corrosion Rate (mm/year)	Current Density (mA/cm^2)
Weld Joint-1	0.608	0.3825	0.0331
Weld Joint-2	0.900	0.2795	0.0240
Weld Joint-3	1.466	0.0902	0.0078

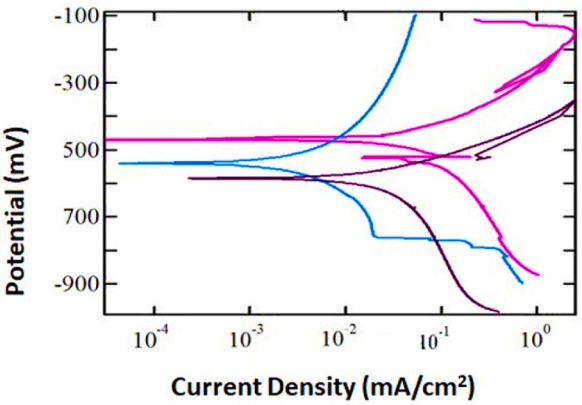

Fig. 12. Potential vs Current Density.

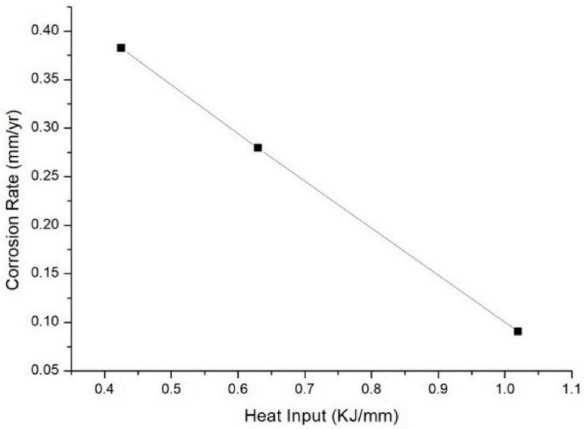

Fig. 13. Heat input vs Corrosion Rate.

Author contribution statement

S. Senthilkumar: Conceived and designed the experiments.
S. Manivannan: Performed the experiments.
R. Venkatesh: Contributed reagents, materials, analysis tools or data.
Karthikeyan M: Analyzed and interpreted the data; Wrote the paper.

Data availability statement

Data will be made available on request.

Additional information

No additional information is available for this paper.

Funding statement

The authors declared that no funding was received for this Research and Publication.

Declaration of competing interest

The authors declare that they have no known competing financial interests or personal relationships that could have appeared to influence the work reported in this paper.

References

[1] J.C. Farrar, A.W. Marshall, Super martensitic stainless steel - overview and weldability, In International Institute of Welding 1 (3) (1988) 423–498.
[2] J.C. Lippold, D.J. Kotecki, Welding Metallurgy and Weldability of Stainless Steels, John Wiley & Sons, Hoboken, NJ, 2005.
[3] G. Rondelli, B. Vicentini, E. andSivieri, Stress corrosion cracking of stainless steels in high-temperature caustic solutions, Corrosion Sci. 39 (1997) 1037–1049.
[4] G. Rondelli, B. Vicentini, Susceptibility of highly alloyed austenitic stainless steels to caustic stress corrosion cracking, Mater. Corrosion 53 (2002) 813–819.
[5] I. Betova, M. Bojinov, et al., Effect of sulphide on the corrosion behaviour of AISI 316L stainless steel and its constituent elements in simulated kraft digester conditions, Corrosion Sci. 52 (2010) 1499–1507.
[6] K. Chasse, S. Raji, P. Singh, Effect of chloride ions on corrosion and stress corrosion cracking of duplex stainless steels in hot alkaline-sulfide solutions, Corrosion 68 (2012) 932–949.
[7] N. Parnian, Failure analysis of austenitic stainless steel tubes in a gas-fired steam heater, Mater. Design 36 (2012) 788–795.
[8] O.M. Alyousif, R. Nishimura, Stress corrosion cracking and hydrogen embrittlement of sensitized austenitic stainless steels in boiling saturated magnesium chloride solutions, Corrosion Sci. 50 (2008) 2353–2359.
[9] K.H. Lo, C.H. Shek, J. Lai, Recent developments in stainless steels, Mater. Sci. Eng. R Rep. 65 (2009) 39–104.
[10] Saravanan P. SrikanthS, P. Govindarajan, et al., Development of lean duplex stainless steels (LDSS) with superior mechanical and corrosion properties on laboratory scale, Adv. Mater. Res. 794 (2013) 714–730.
[11] F. Bonollo, A. Tiziani, P. Ferro, Welding processes, microstructural evolution and final properties of duplex and superduplex stainless steels, in: Duplex Stainless Steels, John Wiley & Sons, Inc., Hoboken, NJ, USA, 2013, pp. 141–159.
[12] A. Kisasoz, S. Gurel, A. andKaraaslan, Effect of annealing time and cooling rate on precipitation processes in a duplex corrosion-resistant steel, Met. Sci. Heat Treat. 57 (2016) 544–547.
[13] Y. Zhang, X. Pang, S. Qu, et al., Discussion of the CO_2 corrosion mechanism between low partial pressure and supercritical condition, Corrosion Sci. 59 (2012) 186–197.

[14] L. Zhang, X. Li, et al., Corrosion and stress corrosion cracking behaviour of X70 pipeline steel in a CO2-containing solution, J. Mater. Sci. Perform. 18 (2009) 319–323.
[15] K. George, S. Nešic, Investigation of carbon dioxide corrosion of mild steel in the presence of acetic acid-Part 1 basic mechanisms, Corrosion 63 (2007) 178–186.
[16] Z. Cui, S. Wu, et al., Study on corrosion properties of pipelines in simulated produced water saturated with supercritical CO2, Appl. Surf. Sci. 252 (2006) 2368–2374.
[17] Y.R. Liu, D. Ye, et al., Effect of heat treatment on microstructure and property of Cr 13 super martensitic stainless steel, J. Iron Steel Res. Int. 18 (11) (2011) 60–66.
[18] S. Kumar, G.P. Chaudhari, S.K. Nath, B. Basu, Effect of preheat temperature on weldability of martensitic stainless steel, Mater. Manuf. Process. 27 (12) (2012) 1382–1386.